Magnetic-field-induced charge redistribution in disordered graphene double quantum dots

Citation: Chiu, K. L., M. R. Connolly, A. Cresti, J. P. Griffiths, G. A. C. Jones, and C. G. Smith. "Magnetic-field-induced charge redistribution in disordered graphene double quantum dots." Phys. Rev. B 92, 155408 (October 2015). © 2015 American Physical Society

As Published: http://dx.doi.org/10.1103/PhysRevB.92.155408

Publisher: American Physical Society

Persistent URL: http://hdl.handle.net/1721.1/99199

Version: Final published version: final published article, as it appeared in a journal, conference proceedings, or other formally published context

Magnetic-field-induced charge redistribution in disordered graphene double quantum dots

K. L. Chiu,[1,2] M. R. Connolly,[1,3] A. Cresti,[4,5] J. P. Griffiths,[1] G. A. C. Jones,[1] and C. G. Smith[1]

[1]*Department of Physics, Cavendish Laboratory, University of Cambridge, Cambridge, CB3 0HE, United Kingdom*

[2]*Department of Physics, Massachusetts Institute of Technology, Cambridge, Massachusetts 02139, USA*

[3]*National Physical Laboratory, Hampton Road, Teddington TW11 0LW, United Kingdom*

[4]*Université Grenoble Alpes, IMEP-LAHC, F-38000 Grenoble, France*

[5]*CNRS, IMEP-LAHC, F-38000 Grenoble, France*

(Received 8 May 2015; revised manuscript received 24 August 2015; published 6 October 2015)

We have studied the transport properties of a large graphene double quantum dot under the influence of a background disorder potential and a magnetic field. At low temperatures, the evolution of the charge-stability diagram as a function of the B field is investigated up to 10 T. Our results indicate that the charging energy of the quantum dot is reduced, and hence the effective size of the dot increases at a high magnetic field. We provide an explanation of our results using a tight-binding model, which describes the charge redistribution in a disordered graphene quantum dot *via* the formation of Landau levels and edge states. Our model suggests that the tunnel barriers separating different electron/hole puddles in a dot become transparent at high B fields, resulting in the charge delocalization and reduced charging energy observed experimentally.

DOI: 10.1103/PhysRevB.92.155408 PACS number(s): 73.63.−b, 72.80.Vp

I. INTRODUCTION

Confining charge carriers in graphene continues to generate interest owing to its customizable electronic properties and compatibility with existing semiconductor device processing [1]. Carbon atoms ^{12}C have low atomic weight and no nuclear spin (except for the ^{13}C isotope), so electronic interactions, such as spin-orbit and hyperfine couplings are expected to be weak in graphene, leading to long electron-spin relaxation times [2]. Over the past decade lithographically defined graphene quantum dots (GQDs) have proved to be a useful platform in which single electrons can be confined and manipulated. A number of experimental advances have been reported, such as charge detection [3], charge relaxation [4], and electron-hole crossover [5], in graphene single quantum dots (GSQDs) and excited states [6], tunable interdot coupling [7], and charge pumping [8] in graphene double quantum dots (GDQDs). More recently, graphene quantum dots on hexagonal boron nitride (hBN) have enabled the influence of potential and edge disorder to be studied separately [9,10]. Magnetic fields are powerful tools for unveiling the nature of a confined Dirac fermion in GQDs. For example, the Fock-Darwin spectrum in the few-electron regime [5] and many-electron regime [11] as well as the Zeeman splitting of spin states [12] in a graphene single quantum dot have been studied. On the other hand, although it is well known that electron transport through graphene nanostructures is strongly affected by electron/hole puddles induced by potential fluctuations [7,13,14], detailed experimental and theoretical studies are lacking to address this issue in GQD transport. In this paper, we study the effect of disorder by investigating the transport properties of a large GDQD device at magnetic fields in which Landau levels (LLs) are expected to form. At a high enough B field, our results suggest that electron/hole puddles in the dot tend to merge together, giving rise to a charge redistribution which can be observed experimentally. Our results are supported by tight-binding quantum simulations, which can be used to describe the charge redistribution in a disordered graphene quantum dot at high magnetic fields and gives deeper insight into our experimental data.

II. COULOMB BLOCKADE MEASUREMENT ON A GRAPHENE DOUBLE DOT AT $B = 0$

Double quantum dots are model systems for investigating the dynamics of electrons in a wide range of semiconductors [15–21]. Charge stability diagrams—obtained by measuring the conductance as a function of the carrier density on each quantum dot—reveal a wealth of information about charging energy, interdot coupling, and cross-gate coupling strength, making them an ideal way to probe charge rearrangements in quantum dots at high magnetic fields. An atomic force microscopy image of the double quantum dot measured in this paper is shown in Fig. 1(a). Our device consists of two lithographically etched (O_2 plasma) graphene islands each with a size of 200×250 nm^2 labeled QD_1 and QD_2 in Fig. 1(a). They are mutually connected to each other by a 90-nm-wide constriction and separately connected to the source/drain leads *via* two 80-nm-wide constrictions, which act as tunnel barriers. Two plunger gates PG1(2) are used to tune the energy levels in $QD_{1(2)}$ whereas three side gates (SG1, SG2, and SG3) are used to tune the tunnel barriers. The doped-silicon backgate (BG) is used to adjust the overall Fermi level.

The measurements were performed in a dilution refrigerator with an electron temperature around 100 mK. In Fig. 1(b), we show the measured differential conductance through DQDs as a function of BG voltage (an ac excitation of $V_{ac} = 20$ μV at 77 Hz from a lock-in amplifier is used) highlighting a region of suppressed current (the so-called transport gap [22]) separating the hole from the electron transport regime. At a backgate voltage within the transport gap [$V_{BG} = 8.61$ V, see arrow in Fig. 1(b)] we measure the dc current through the DQD as a function of V_{PG1} and V_{PG2} for a series of applied dc biases as shown in Fig. 1(c) for $V_b = 400$ μV, (d) for $V_b = 1$ mV, and (e) for $V_b = 2$ mV, respectively.

As expected, the current in the stability diagram evolves from triple points into bias-dependent triangles when the bias is increased. The horizontal and vertical measures of the honeycomb cell ΔV_{PG1} and ΔV_{PG2} [Fig. 1(d)] give the capacitances between gate PG1 and QD_1 $C_{g1} \approx e/\Delta V_{PG1} =$

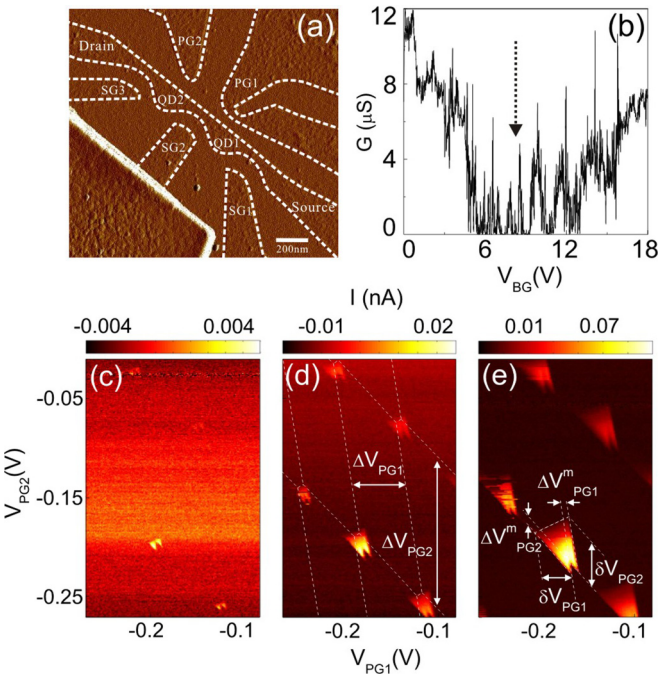

FIG. 1. (Color online) (a) Atomic force micrograph of the double quantum dot device measured in this paper. (b) Measurement of the differential conductance through the DQD for varied backgate voltages. Data collected at $V_{ac} = 200\ \mu$V and $T = 1.4$ K. Current through the DQD as a function of V_{PG1} and V_{PG2} measured in a dilution refrigerator at $T = 100$ mK with applied dc biases (c) $V_b = 400\ \mu$V, (d) $V_b = 1$ mV, and (e) $V_b = 2$ mV. The position of the triple points can be determined at low bias [see (c)], whereas at high bias the triple points evolve into triangles [see (d) and (e)].

2.77 aF and between gate PG2 and QD_2 $C_{g2} \approx e/\Delta V_{PG2} = 1$ aF. Also the charging energies $E_{C1} = \alpha_1 \Delta V_{PG1} = 2.57$ and $E_{C2} = \alpha_2 \Delta V_{PG2} = 4.77$ meV are obtained using the voltage-energy conversion factor $\alpha_{1(2)} = eV_b/\delta V_{PG1(2)}$ extracted from the bias triangle as shown in Fig. 1(e). The difference in charging energies reflects the fact that the sizes of the dots are not equal and can be justified if the tunnel barriers defined by local disorder potential modify the size of the GQDs [7,13]. Within this picture, electrons from the source reservoir enter through a large localized state in QD_1 (E_{C1} is small) to a small localized state in QD_2 (E_{C2} is large) and then exit through the drain reservoir. Finally, the interdot coupling energy can be determined from the splitting of the triangles as shown in Fig. 1(e): $E_{Cm} = \alpha_1 \Delta V^m_{PG1} = 0.29$ meV.

III. CHARGE STABILITY DIAGRAM IN A PERPENDICULAR MAGNETIC FIELD

The charge distribution in the QDs can be investigated by looking at how the charge stability diagram evolves under the influence of the magnetic field. Figure 2(a) shows the evolution of a region of the stability diagram, measured at $T = 100$ mK, $V_{BG} = 8.61$ V, and $V_b = -1$ mV for perpendicular magnetic fields ranging from 4 to 10 T. Note that the voltage ranges on the x-y axes of Figs. 2(a) and 2(b) are chosen to be the same in each panel. We have studied the stability diagram in a wide energy range and here only focus on four typical triple points for simplicity. The first observation is the field-dependent change in the dimensions of the honeycomb, which is highlighted by the dotted hexagonal outlines in Fig. 2(a) and is most pronounced from $B = 7$ to $B = 10$ T, indicating the variation in the capacitances C_{g1} and C_{g2}. In addition, the closeups of the triangle in the bottom of each honeycomb, as shown Fig. 2(b), display a change in $\delta V_{PG1(2)}$ and $\Delta V^m_{PG1(2)}$, implying that the conversion factors $\alpha_{1(2)}$ and interdot coupling energy E_{Cm} also change with the B field. It is worth noting that the size of the triangle varies in the same honeycomb (i.e., $B = 7$ and 8 T), indicating the precise size of the localized state can change over a small range of gate voltage. The extracted charging energy of each dot (E_{C1} and E_{C2}) and the interdot coupling energy (E_{Cm}) are shown in Figs. 2(c) and 2(d), respectively. The QD charging energies remain roughly unvaried ($E_{C1} \approx 3$ and $E_{C2} \approx 6$ meV) from $B = 4$ to $B = 6$ T then show a decreasing tendency from $B = 7$ T to higher fields. From $B = 4$ to $B = 10$ T, the percentage change in E_{C2} (42%) is larger than that in E_{C1} (27%). By contrast, the interdot coupling energy shows a monotonic increase with the field from 4 to 10 T. Our results suggest that both dots increase their "effective" size at high B fields, which reflects on the decreasing charging energies.

IV. MODEL AND SIMULATION

It is well known that the presence of charged impurities in the SiO_2 substrate [23,24] or surface ripples [25] can induce electron-hole puddles with a size of tens of nanometers in exfoliated graphene flakes. This aspect considerably affects the electronic and transport properties of graphene around the Dirac point, and as we will show, it plays a key role in our case. To take this into account, we consider a varying background potential V in a model QD as shown in Fig. 3(a) where V fluctuates from positive (blue) to negative (red) passing from $V = 0$ (green). If V varies slowly, in each region of a large dot the energy bands will approximately correspond to the shifted energy bands of two-dimensional graphene as represented in Fig. 3(b) for zero (left panel) and high (right panel) magnetic fields. At $B = 0$ T, a gap is introduced to include the quantum confinement effects due to the dot. This gap progressively reduces at the high B field along with the formation of Landau levels. Depending on the backgate and background potentials, the Fermi energy E_F (here set to 0) and Dirac point can have locally different relative positions as indicated by the dashed lines in the left panel of Fig. 3(b). The sign and strength of V determine the nature (electron or hole) of the puddles and their DOS. We first consider the case of $B = 0$. For the $V \ll 0$ ($V \gg 0$) regions, the Fermi energy corresponds to level 1 (5) in Fig. 3(b). As the level is far above (below) the charge neutrality point, it gives rise to the electron (hole) puddles with high DOS as shown in Fig. 3(c). In the region where $V < 0$ ($V > 0$), the Fermi energy corresponds to level 2 (4) and results in electron (hole) puddles with low DOS. In the region around $V = 0$ corresponding to the energy gap, the DOS is very low or 0. These regions [the green region in Fig. 3(c)] separate the puddles and can make the transport diffusive [26].

In the presence of high magnetic fields, due to the formation of LLs, part of the levels around the gap tends to the 0th

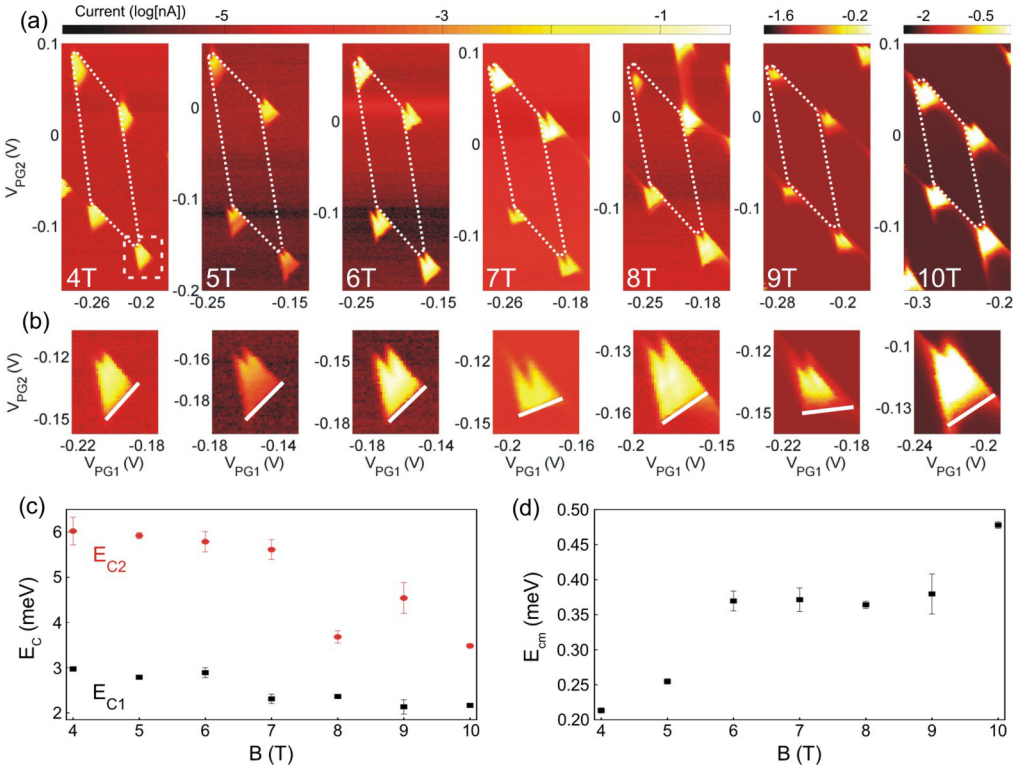

FIG. 2. (Color online) (a) The evolution of the charge-stability diagram (taken at $T = 100$ mK, $V_{BG} = 8.61$ V, and $V_b = -1$ mV) under the influence of a perpendicular magnetic field from 4 to 10 T. (b) Closeup of the triangle in the lowest position of each panel as highlighted by the dashed square in the leftmost panel of (a). Note that the voltage ranges on the x-y axes of (a) and (b) are chosen to be the same in each panel. (c) The charging energies of the QDs as a function of the B field. (d) The interdot coupling energy as a function of the B field. Note that in order to consider the distortion of the triangle at certain B fields (e.g., $B = 7$ and 9 T), we use the right tip and the left tip of each triangle to doubly define the shape of the triangle. We take the average of both fittings (meaning the triangle shape determined by the left tip and the right tip) to extract the data points, and the error bar is determined by the difference between the two fittings.

Landau level, thus reducing the gap. The other part rises, thus approaching the higher LLs as shown in the right panel of Fig. 3(b) where also the dispersive magnetic edge states are represented. In the low-field regime, the LLs are far from being fully established, and the DOS in the dot is low. However, the edge channels start developing with opposite chirality for electron and hole puddles as indicated by arrows in Fig. 3(d). At the high magnetic field, the LL_0 is well developed with the consequent closing of the band gap. Therefore, in the $V = 0$ region the DOS is expected to increase and result in the development of nonchiral channels connecting the puddles as shown in the yellow region in Fig. 3(e). At the same time, the other LLs start developing together with the chiral magnetic edge channels. In this regime, the DOS decreases in the bulk of the puddles whereas it increases at their edges. Electron transport through the dot is not confined in a particular puddle but can be delocalized in the dot through flowing in both the chiral edge channels (red or blue arrows) and the nonchiral channels (yellow region).

In order to validate this picture, we performed numerical simulations of a QD with a radius of $R = 47.5$ nm and a background potential consisting of two regions with $V > 0$ (81 meV) and $V < 0$ (−66 meV), which determine the presence of a hole puddle and an electron puddle as shown in Fig. 4(a). Note that in order to reduce the computational burden, we choose to simulate a dot that is smaller than the real ones and with a simplified background potential. However, the result we got is representative of a larger dot with more complicated background potential. The dot is described by a first-neighbor tight-binding Hamiltonian with a single p_z orbital *per* atom and coupling parameter −2.7 eV. For more details on the Green's function formalism adopted for the simulations, refer to Ref. [27]. The calculated DOS of the dot is shown in Figs. 4(b)–4(f) in arbitrary units. As expected, at low B (0 and 0.8 T) the DOS is low where $V = 0$ and higher for larger $|V|$. As B increases (2.8 T), the DOS decreases a little in the center of the electron/hole puddles, and it increases along the edge due to the progressive developing of magnetic edge states [Fig. 4(d)]. Note the presence of a very high DOS region at the border of the dot. They correspond to zigzag edge sections where very localized states appear [28]. At a higher B field, we observe the presence of high DOS in the $V = 0$ region, which corresponds to the LL_0, and the rise of edge states around the dot. The higher the field is, the larger the DOS is in the $V = 0$ and edge regions as can be seen for $B \geqslant 4.4$ T in Figs. 4(e) and 4(f).

The simulated background spectral current distribution (which corresponds to the spatial distribution of the conductive channels) [27] in the dot is shown in Figs. 4(g)–4(j). At the low magnetic field ($B \leqslant 0.8$ T) the current is mainly concentrated in the high $|V|$ regions, and the $V = 0$ region seems to act as a barrier between the two puddles. At a slightly higher field

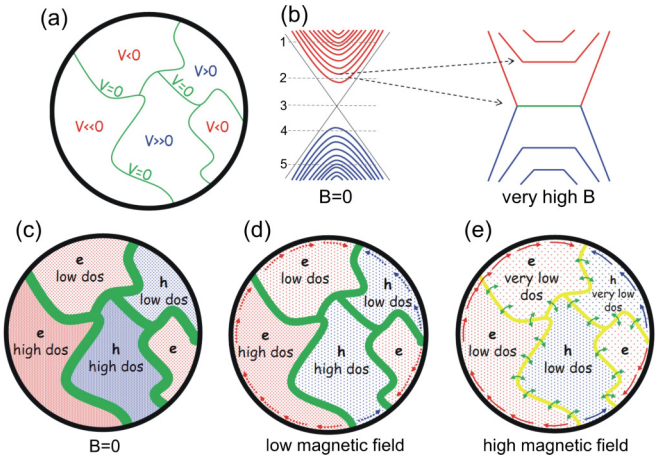

FIG. 3. (Color online) (a) Example of potential distribution in a large disordered quantum dot. (b) Left panel: Schematic band structure of a GQD in zero magnetic field. Right panel: in a high magnetic field. The red lines denote the electronlike levels, and the blue lines denote the holelike levels. The black solid lines indicate the Dirac conelike dispersion. (c)–(e) Expected density of state (DOS) distribution in the dot at zero field, low magnetic field, and high magnetic field, respectively.

($B = 2.8$ T) the current starts tending to the $V = 0$ region due to the progressive closing of the energy gap. At high fields ($B \geqslant 4.4$ T), we observe the current flowing along the chiral magnetic edge states of the dot and along the nonchiral $V = 0$ region where the gap is now closed. In this regime, the current is delocalized in the dot, and a charge rearrangement can be seen compared to the case at low B fields. Note that the more fractured the disorder potential is (meaning more existing electron/hole puddles), the more pronounced the charge delocalization effect will be at high fields.

V. DISCUSSION

As the backgate voltage ($V_{BG} = 8.61$ V) where all the measurements were carried out is near the charge neutrality point, it is expected the background potential fluctuations will play a role and give rise to electron-hole puddles formed in the QDs [24,29]. In this situation, our model can be readily adapted to explain the data. Due to the closing of the energy gap at high enough magnetic fields, at the $V = 0$ region, the DOS is high and develops nonchiral channels which connect the puddles as sketched in Fig. 3(e). Hence, the current can flow through the puddles *via* crossing the high DOS nonchiral channels at the interface, thus making electrons no longer confined in a particular puddle but delocalized in a larger puddle, resulting in a smaller charging energy. Here we point out that the field has to be high enough for the LLs and edge states to be fully developed to close the energy gap. The threshold B field for this to happen in a GSQD with a relatively smaller size (50-nm diameter) is around 10 T [5]. As a result, the change in charging energies in our case is most pronounced from $B = 6$ to $B = 10$ T for QD_1 and from $B = 7$ to $B = 10$ T for QD_2 as shown in Fig. 2(c). The threshold B field for QD_2 is higher owing to its larger charging energy (smaller puddle) in which the magnetic length $\ell_B = \sqrt{\hbar/eB}$ has to be comparable or

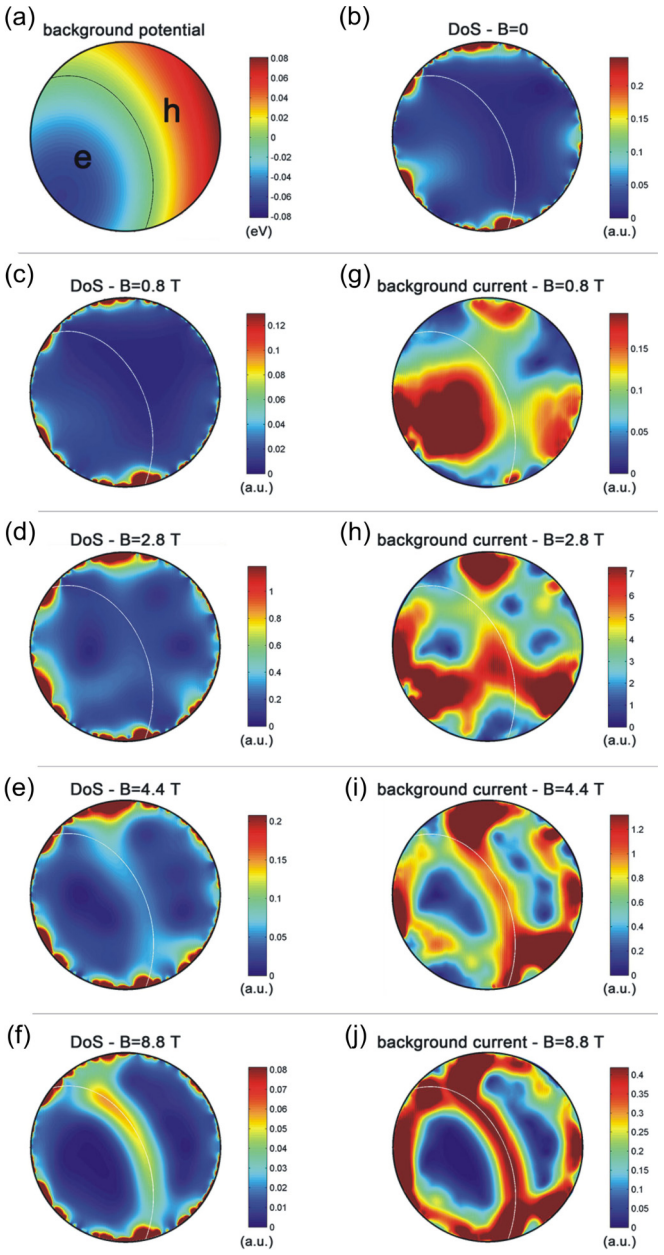

FIG. 4. (Color online) (a) Potential distribution in a quantum dot with $R = 47.5$ nm. The black line in the potential profile indicates the region where the potential is $V = 0$. (b)–(f) Calculated local DOS in the dot at different magnetic fields. (g)–(j) Calculated current distribution in the dot at different magnetic fields.

even smaller than the puddle size. The magnetic length for $B = 7$ T is around 9 nm, implying the size of the puddle in the dot is around (or more than) twice the critical magnetic length, in good agreement with the puddle size (20 nm) measured in graphene [23]. In addition, we observed the change in E_{C2} from $B = 4$ to $B = 10$ T is larger than that in E_{C1}. This is expected since E_{C1} is smaller than E_{C2}, indicating electrons tunnel through a larger localized state in QD_1 and a smaller localized state in QD_2. In other words, the disorder potential in QD_2 is more fractured than that in QD_1. Therefore, at a high B field the charge delocalization effect is more pronounced in QD_2 than that in QD_1, giving rise to the larger B-dependent

charging energy in QD_2. Here we note that the GQD has to be large for the substrate disorder to play an important role, which may be the reason that the decreasing charging energy with the B field is not observed in other relatively smaller GQDs with large edge-to-bulk ratios [3,5] or GQDs on hBN [10] where substrate disorder is less important. The increasing interdot coupling energy may be also understood as the charges rearranging from the center of the puddles to the edge of the dot [see Figs. 4(g)–4(j)]. This scenario depends on the progressively formed edge state with increasing B field and can be observed in the whole range of the B field [Fig. 2(d)].

A more recent study of graphene nanoribbons (GNRs) on the hBN substrate has indicated that the localized states may also extend into the leads of the device, giving rise to smaller charging energies than expected from the geometry of GNRs alone [30]. However, two conditions are crucial for this effect to be seen. One is the substrate disorder has to be much weaker than the edge disorder, and the other is the edge-to-bulk ratio of the device has to be large enough for the edge to play an important role. Transport in GQDs on hBN is dominated by the edge roughness for QDs with diameters less than 100 nm [9]. Each condition is met by their relatively small GNR (30 nm × 30 nm) on hBN, thus the edge disorder is strong enough to localize the electron wave function along the edge to the leads. On the contrary, our large dot (and the tunnel barrier GNR) with a smaller edge-to-bulk ratio should diminish the influence of the rough edges on overall transport, meaning localization along the edge still happens, but transport is dominated by bulk contributions. Therefore, we argue that the charge redistribution (based on substrate disorder) in our QDs is the main factor that leads to a variation in the effective dots' area and contributes to the decreasing charging energies in magnetic fields.

The effect of disorder can be also seen in Fig. 5 where a stability diagram measured in different cool downs of the device at B fields (a) 3.2 T, (b) 3.8 T, and (c) 4.4 T is presented. The triangle shape first distorts at $B = 3.2$ T, then splits into two separated ones [Fig. 5(b)], and then moves further apart and forms an additional row of triangles [Fig. 5(c)]. We attribute this newly appearing triangle to the formation of a localized state in a magnetic field, which is capacitively coupled to the original dots [31,32]. A schematic is shown in Figs. 5(d) and 5(e) to address such a scenario. When a localized state is formed in a magnetic field, while the gate voltage is swept, it can add or subtract charges discretely to the parasitic dot, thus altering the entire environment abruptly and unexpectedly. The fact that the splitting occurs on both gate spaces suggests the localized state can affect two dots in a similar way, implying its location is in the central GNR [Fig. 5(d)]. The new dot acts as a gate which will shift the triple points in the charge-stability diagram, consequently, leading to an additional row of triangles being added adjacent to the original ones.

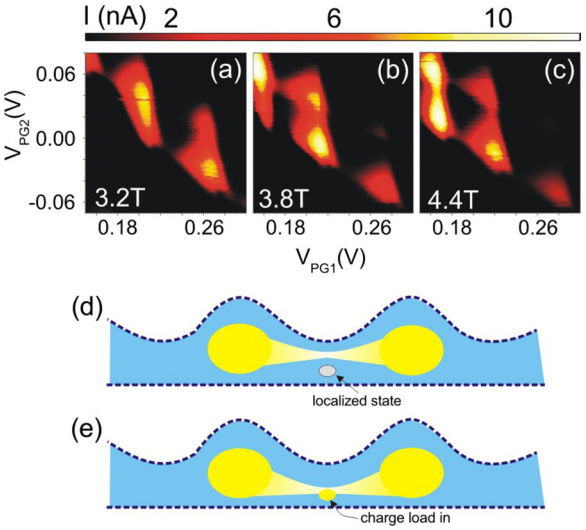

FIG. 5. (Color online) The charge-stability diagram measured at $V_{BG} = 9$ V and $V_b = 1$ mV in (a) $B = 3.2$ T, (b) $B = 3.8$ T, and (c) $B = 4.4$ T showing a formation of an additional dot under the influence of a magnetic field and strongly coupled to the original dots. (d) Graphic illustration of an effect of a localized state formed in magnetic fields. (e) Same as (d) but with a charge added into the localized state. It capacitively couples to the original dots and forces the DQD to reconstruct its wave function.

VI. SUMMARY

To summarize, we have fabricated and studied the magneto-transport properties of a large GDQD device. In different cool downs, we observed a honeycomb pattern which is typical of charge-stability diagrams for a DQD system. We studied the evolution of the charge-stability diagram under the influence of a B field up to 10 T. The charging energy and the interdot coupling energy show different dependences with the B field, suggesting the size of both dots become larger in a high field. Our interpretation is supported by numerical simulations in which we show the confined charges in the puddles of GQDs can be redistributed from the bulk to the edge through the formation of LLs and edge states. At a high enough B field, due to the closing of the energy gap, electrons are delocalized *via* crossing the nonchiral channels connecting different puddles, resulting in a smaller charging energy.

ACKNOWLEDGMENT

This work was financially supported by the European GRAND project (ICT/FET, Contract No. 215752) and EPSRC.

[1] A. K. Geim and K. S. Novoselov, Nature Mater. **6**, 183 (2007).
[2] D. Huertas-Hernando, F. Guinea, and A. Brataas, Phys. Rev. Lett. **103**, 146801 (2009).
[3] J. Guttinger, Appl. Phys. Lett. **93**, 212102 (2008).
[4] C. Volk, C. Neumann, S. Kazarski, S. Fringes, S. Engels, F. Haupt, A. Müller, and C. Stampfer, Nat. Commun. **4**, 1753 (2013).

[5] J. Guttinger, C. Stampfer, F. Libisch, T. Frey, J. Burgdorfer, T. Ihn, and K. Ensslin, Phys. Rev. Lett. **103**, 046810 (2009).
[6] F. Molitor, H. Knowles, S. Droscher, U. Gasser, T. Choi, P. Roulleau, J. Guttinger, A. Jacobsen, C. Stampfer, K. Ensslin *et al.*, Europhys. Lett. **89**, 67005 (2010).
[7] X. L. Liu, D. Hug, and L. M. K. Vandersypen, Nano Lett. **10**, 1623 (2010).
[8] M. R. Connolly, K. L. Chiu, S. P. Giblin, M. Kataoka, J. D. Fletcher, C. Chua, J. P. Griffiths, G. A. C. Jones, V. I. Fal'ko, C. G. Smith and T. J. B. M. Janssen, Nat. Nanotechnol. **8**, 417 (2013).
[9] S. Engels, A. Epping, C. Volk, S. Korte, B. Voigtlander, K. Watanabe, T. Taniguchi, S. Trellenkamp, and C. Stampfer, Appl. Phys. Lett. **103**, 073113 (2013).
[10] A. Epping, S. Engels, C. Volk, K. Watanabe, T. Taniguchi, S. Trellenkamp, and C. Stampfer, Phys. Status Solidi B **250**, 2692 (2013).
[11] K. L. Chiu, M. R. Connolly, A. Cresti, C. Chua, S. J. Chorley, F. Sfigakis, S. Milana, A. C. Ferrari, J. P. Griffiths, G. A. C. Jones *et al.*, Phys. Rev. B **85**, 205452 (2012).
[12] J. Guttinger, T. Frey, C. Stampfer, T. Ihn, and K. Ensslin, Phys. Rev. Lett. **105**, 116801 (2010).
[13] C. Volk, S. Fringes, B. Terres, J. Dauber, S. Engels, S. Trellenkamp, and C. Stampfer, Nano Lett. **11**, 3581 (2011).
[14] F. Amet, J. R. Williams, A. G. F. Garcia, M. Yankowitz, K. Watanabe, T. Taniguchi, and D. Goldhaber-Gordon, Phys. Rev. B **85**, 073405 (2012).
[15] R. Hanson, L. P. Kouwenhoven, J. R. Petta, S. Tarucha, and L. M. K. Vandersypen, Rev. Mod. Phys. **79**, 1217 (2007).
[16] W. G. van der Wiel, S. De Franceschi, J. M. Elzerman, T. Fujisawa, S. Tarucha, and L. P. Kouwenhoven, Rev. Mod. Phys. **75**, 1 (2002).
[17] A. Pfund, I. Shorubalko, R. Leturcq, and K. Ensslin, Appl. Phys. Lett. **89**, 252106 (2006).
[18] M. D. Schroer, K. D. Petersson, M. Jung, and J. R. Petta, Phys. Rev. Lett. **107**, 176811 (2011).
[19] S. J. Chorley, G. Giavaras, J. Wabnig, G. A. C. Jones, C. G. Smith, G. A. D. Briggs, and M. R. Buitelaar, Phys. Rev. Lett. **106**, 206801 (2011).
[20] S. Pecker, F. Kuemmeth, A. Secchi, M. Rontani, D. C. Ralph, P. L. McEuen, and S. Ilani, Nat. Phys. **9**, 576 (2013).
[21] F. A. Zwanenburg, A. S. Dzurak, A. Morello, M. Y. Simmons, L. C. L. Hollenberg, G. Klimeck, S. Rogge, S. N. Coppersmith, and M. A. Eriksson, Rev. Mod. Phys. **85**, 961 (2013).
[22] C. Stampfer, J. Guttinger, S. Hellmuller, F. Molitor, K. Ensslin, and T. Ihn, Phys. Rev. Lett. **102**, 056403 (2009).
[23] Y. Zhang, V. W. Brar, C. Girit, A. Zettl, and M. F. Crommie, Nat. Phys. **5**, 722 (2009).
[24] J. Martin, N. Akerman, G. Ulbricht, T. Lohmann, J. H. Smet, K. von Klitzing, and A. Yacoby, Nat. Phys. **4**, 144 (2008).
[25] A. Deshpande, W. Bao, F. Miao, C. N. Lau, and B. J. LeRoy, Phys. Rev. B **79**, 205411 (2009).
[26] Q. Li, E. H. Hwang, and S. Das Sarma, Phys. Rev. B **84**, 115442 (2011).
[27] A. Cresti, G. Grosso, and G. P. Parravicini, Eur. Phys. J. B **53**, 537 (2006).
[28] K. Nakada, M. Fujita, G. Dresselhaus, and M. S. Dresselhaus, Phys. Rev. B **54**, 17954 (1996).
[29] M. R. Connolly, K. L. Chiou, C. G. Smith, D. Anderson, G. A. C. Jones, A. Lombardo, A. Fasoli, and A. C. Ferrari, Appl. Phys. Lett. **96**, 113501 (2010).
[30] D. Bischoff, F. Libisch, J. Burgdörfer, T. Ihn, and K. Ensslin, Phys. Rev. B **90**, 115405 (2014),
[31] J. Guttinger, C. Stampfer, T. Frey, T. Ihn, and K. Ensslin, Nanoscale Res. Lett. **6**, 253 (2011).
[32] D. Wei, H.-O. Li, G. Cao, G. Luo, Z.-X. Zheng, T. Tu, M. Xiao, G.-C. Guo, H.-W. Jiang, and G.-P. Guo, Sci. Rep. **3**, 3175 (2013).